Diamond & Related Materials 157 (2025) 112493

Contents lists available at ScienceDirect

Diamond & Related Materials

journal homepage: www.elsevier.com/locate/diamond

Effect of reinforcement amount on the microstructural and mechanical properties of mechanically alloyed graphene nanoplatelet reinforced Al-3.5 wt% Cu composites

Sıddıka Mertdinç-Ülküseven [a,*], İlayda Süzer [a], Ahmet Kasım Ürper [a], Alper İbrahim Çelik [a], Doruk Tuncer Baci [a], Kerem Alper Güraslan [a], M. Lütfi Öveçoğlu [a,b], Duygu Ağaoğulları [a,*]

[a] Istanbul Technical University, Faculty of Chemical and Metallurgical Engineering, Metallurgical and Materials Engineering Department, Particulate Materials Laboratories (PML), Graphene & 2D Materials Laboratory, 34469 Maslak, Istanbul, Türkiye
[b] MEF University, Department of Mechanical Engineering, 34396 Sarıyer, Istanbul, Türkiye

ARTICLE INFO

Keywords:
Al—Cu alloys
Metal matrix composites
Graphene nanoplatelets (GNPs)
Mechanical alloying
Pressureless sintering
Mechanical properties
Microstructural properties

ABSTRACT

In this study, various amounts (0.25, 0.5, 0.75, 1, and 2 wt%.) of graphene nanoplatelets (GNPs) reinforced Al-3.5 wt% Cu metal matrix composites were produced using powder metallurgy processes consisted mechanical alloying and pressureless sintering. To compare the properties of the sintered composites, as-blended and 4 h mechanically alloyed powders were sintered to yield Al-3.5 wt% Cu matrix alloys. The microstructural, thermal and mechanical properties were examined using relevant characterization techniques. The formation of Al_2Cu phase was detected at all XRD patterns of the sintered samples other than matrix and reinforcement phases. Mechanically alloyed powders exhibit the equiaxed particle morphology compared to the as-blended ones, their mechanical properties were found better than as-blended and sintered samples. Additionally, mechanical alloying led to the dispersion of GNP reinforcements into the Al—Cu matrix. The highest hardness value (around 153 HV) was obtained for 2 wt% GNP reinforced composite. The highest wear resistance was recorded for 1 wt% GNP reinforced composite with 2.07 ± 0.2 $mm^3/N.m \times 10^{-3}$ wear rate. Additionally, composites' compressive strength improved with adding 1 wt% GNP (~68.5 MPa). The good dispersion of the optimum amount of GNP's via mechanical alloying provide to obtain preferable mechanical properties.

1. Introduction

Graphene that consists of sp^2 hybridized carbon atoms has two dimensional (2D) honeycomb lattice structure [1–3]. Lightweight (planar density of 0.77 mg/m^2), high transparency, high electrical and thermal conductivity, and high toughness, and strength are some excellent properties of graphene [4]. Graphene nanoplatelets (GNPs) are consisted of multiple graphene layers (10–30 graphene sheets) which their thickness varies between 0.7 and 100 nm [5–7]. GNPs and multi-layer graphene are cheaper and easier to produce than the single-layer graphene; also both of them have similar superior properties to single-layer graphene [5,7,8]. Low density, great thermal, and electrical conductivity, high hardness, large surface area and high aspect ratio are some of the remarkable properties of planar-shaped GNPs [9,10]. Due to their superior physical, thermal, electrical, and mechanical features, GNPs are preferred as reinforcement materials for metals, ceramics and polymers to constitute composites [5,7]. Among the GNPs reinforced composites, aluminum-based metal matrix composites have been worked on a lot. Al-based metal matrix composites are favored by the automotive, marine, defense, electronic, and aerospace industries for their superior performance due to their light weight, high strength, wear and corrosion resistance, low thermal expansion, etc [11–15]. Among the Al-based materials, Cu could be added as an alloying element to improve mechanical properties via the formation of Cu-rich intermetallic phases such as metastable Al_2Cu [16,17]. According to the Al—Cu phase diagram, the solubility limit of Cu in Al at a temperature of about 548 °C is ~5.65 wt% [18]. The in-situ formed Al_2Cu phase prevents the dislocation movements, causes precipitation hardening and improves the alloy's strength, corrosion resistance, and hardness [19–23].

Homogeneous dispersion of GNPs and interfacial bonding between GNP and matrix are essential, especially in improving the mechanical properties of composites [24,25]. Because the homogeneously dispersed

* Corresponding authors.
E-mail addresses: mertdinc@itu.edu.tr (S. Mertdinç-Ülküseven), bozkurtdu@itu.edu.tr (D. Ağaoğulları).

https://doi.org/10.1016/j.diamond.2025.112493
Received 31 October 2024; Received in revised form 20 May 2025; Accepted 28 May 2025
Available online 28 May 2025

GNP phase led to grain refinement and decreased dislocation mobility. Additionally, stress/load transfer to well-dispersed GNP and mechanical properties of the composites are improved [24]. It should be also noted that GNP has been a remarkable material since its discovery due to its 2D honeycomb structure. In addition, it has become an attractive reinforcement material that can be preferred in many application areas thanks to its ability to improve both mechanical and thermal properties even with the smallest amount of reinforcement [26,27].

Although many Al-based composites are produced in solid and liquid states, mechanical alloying (MA), one of the solid phase production techniques, gains attention in terms of homogeneous distribution of reinforcements into the matrix. Room-temperature solid-state powder metallurgy method named MA can be used to incorporate or disperse reinforcement materials in a metal matrix, resulting in a homogenous particle distribution in the microstructure caused by superior mechanical properties [27–30]. Rashidi et al. [31] mentioned that the GNPs embedded in Al matrix via high-energy ball milling increased the dispersion of phases. For instance, Zheng et al. [32] synthesized 5 vol% GNP reinforced Al composites via continuous high-energy ball milling, subsequent spark plasma sintering and hot extrusion. Zheng et al. [32] mentioned that the improvement in mechanical properties via GNP reinforcement is related to the load transfer capacity of the homogeneously distributed reinforcement particles. Rashad et al. [33] investigated the mechanical properties of GNP-reinforced pure Al composites, and they showed the hardness and tensile strength improvements. Zhang et al. [24] achieved the 115.1 % hardness increment with addition of 1 vol% graphene nanosheets into Al matrix. Pérez-Bustamante et al. [10] showed that both GNP addition (up to 1 wt%) and milling time (1, 3, and 5 h) improved the hardness of sintered materials. Akçamlı et al. [34] enhanced hardness to 199.4 ± 1.88 HV and reduced the wear volume loss to 0.4476 mm^3 with the addition of 0.5 wt% GNP into Al matrix.

Most of the GNP reinforced Al-based composites have been studied with only pure Al matrix. There are a few studies focused on the Al—Cu based matrix. Zheng et al. [35] fabricated GNP-reinforced Al2024 (consisted Al, Cu, Mg, and Si) via thermomechanical treatment. Al-Cu-Al_2O_3/graphene nanocomposites were synthesized by El-Kady et al. [36], and they declared the increase in corrosion resistance with the addition of graphene and Al_2O_3. Powder metallurgy assisted Al2024/1 wt% TiC/1 wt% GNPs nanocomposites is another related study that shows the improvement in compression resistance [37]. Another study focused on Al2024-based matrix reinforced with in-situ formed SiC and GNP and reported increase in the thermal conductivities of composites [13]. Süzer et al. [38] synthesized GNP reinforced (0.1–1 wt%) recycled Al composites with ~1.16 GPa average hardness and they obtained the highest wear resistance (with ~0.00225 mm^3/Nm wear rate) for 0.7 wt % GNP reinforced and recycled Al composite.

In the presented study, various amounts (0.25, 0.5, 0.75, 1, and 2 wt %.) of GNP-reinforced Al-3.5 wt% Cu matrix composites were produced using powder metallurgy routes consisting mechanical alloying, cold-pressing and pressureless sintering. Although there are many studies related to GNP-reinforced Al-based composites, manufacturing of GNP-reinforced Al-3.5 wt% Cu composites using powder metallurgy routes is declared first time to the best of our knowledge. To compare the properties of the composites and show the effect of ball milling and GNP addition, non-milled and non-reinforced samples were also manufactured. The sintered composites were investigated based on their physical, microstructural and mechanical properties. Therefore, the obtained results contributed to the literature by showing the effect of GNP reinforcement on the Al-3.5 wt% Cu matrix.

2. Experimental procedure

Aluminum (Al, Alfa Aesar, 99 % purity, ≤ 44 μm), copper (Cu, Alfa Aesar, 99 % purity, ≤ 44 μm) and graphene nanoplatelets (GNPs, Alfa Aesar, <10 nm) are used as raw materials. XRD patterns of raw materials were presented in Fig. 1a. Existence of pure Al (ICDD Card No: 01–089-2837, Bravais Lattice: face-centered cubic, a = b = c = 0.405 nm), Cu (ICDD Card No: 01–089-2838, Bravais Lattice: face-centered cubic, a = b = c = 0.361 nm) and C (ICDD No: 00–026-1076, Bravais lattice: hexagonal, a = b = c = 2.456 nm) phases were seen from their XRD patterns. Additionally, Raman spectra and SEM images of GNPs are given in Fig. 1b and c. Raman spectrum confirms the graphene content based on I_D/I_G value (0.5), and SEM images also show their agglomerated platelet morphologies.

3.5 wt% Cu and 96.5 wt% Al powders were weighed and blended using a WAB T2C Turbula blender for 30 min to produce as-blended powders. Then, both Al-3.5 wt% Cu powders and various amounts (0.25, 0.5, 0.75, 1 and 2 wt%) GNPs reinforced Al-3.5 wt% Cu powder mixtures were filled into milling vials into a MBRAUN glovebox under Argon (Ar, Linde, 99.999 % purity) atmosphere. Additionally, 2 wt% stearic acid ($C_{18}H_{36}O_2$, ZAG, 99.5 % purity) was added into each milling batch as a process control agent against cold welding of ductile materials during milling. Stainless steel milling vials and balls were preferred for milling studies; also, the ball-to-powder weight ratio was used as 7:1. Prepared milling vials were placed into a high-energy ball mill (SPEX 8000D Mixer/Mill) and milled for 4 h. After milling, obtained powders consolidated using a uniaxial hydraulic press (MSE MP-0710). Cold-pressed samples were subjected to debinding process using a Protherm PTF 14/105/450 tube furnace with a quartz reactor that heated to 420 °C (heating and cooling rate of 2 °C/min) for 2 h under Ar gas flow. During the debinding step, stearic acid was removed from the samples. Then, samples were sintered at 550 °C (heating and cooling rate of 10 °C/min) for 2 h under Ar gas flow using the similar tube furnace at debinding. Powder preparation, mechanical alloying, pressing, debinding and sintering process to obtain sintered products are illustrated in Fig. 2. The compositions of the prepared samples with their abbreviations are shown in Table 1.

The phase identifications of mechanically alloyed powders and sintered composites were conducted using Bruker D8 Advanced Series X-ray powder diffractometer (XRD) using CuK_α ($\lambda = 0.154$ nm) radiation. The data of the XRD were also taken in the range of 10–90° with 2°/min rate and 0.02° step size. The International Center for Diffraction Data® (ICDD) powder diffraction database was used for phase identifications. Average crystallite sizes and lattice strains of powders were calculated using Bruker-AXS TOPAS software. The morphologies of the powders, sintered composites and wear tracks were analyzed using Thermo-Scientific Quattro S and JEOL-6000 Neoscope scanning electron microscope (SEM) equipped with energy dispersive spectroscopy (EDS). Thermal properties of the powders were determined using a Linseis PT1600 differential scanning calorimeter (DSC) by heating up to 700 °C with 10 °C/min heating/cooling rate using alumina crucibles under Ar atmosphere. Densities of the sintered products measured using Archimedes' method. The microhardness test was performed using Shimadzu HMV microhardness tester (with Vickers indenter). After the 30 successful indentations, average hardness values were calculated with their standard deviations. First, different loads (25 g, 50 g, 100 g, 200 g, 300 g, 500 g, 1 kg, 2 kg) were applied at hardness test and traces of hardness indenters taken by Carl Zeiss Axiolab-5 optical microscope were examined to determine the appropriate load. After all samples were analyzed, a test load of 25 g (245.2 mN) was determined as optimum one. The wear performance of the sintered samples was determined using a reciprocating wear tester (Tribotechnic oscillating tribotester tribometer) using a 100Cr6 steel ball (ϕ 6 mm) under a 4 N load for a 25,000 mm total sliding distance with 5 mm/s sliding speed. Based on the wear tracks, wear volume losses were calculated using 2D contact surface profilometer (Veeco Dektak-6 M). The wear tracks were monitored using a Zeiss Stereo Discovery V.20 stereo microscope. Additionally, Shimadzu Autograph AGS-J was used for compression tests (loading rate of 0.18 mm/min). Average compression results were determined after three successful compression tests conducted for each sample.

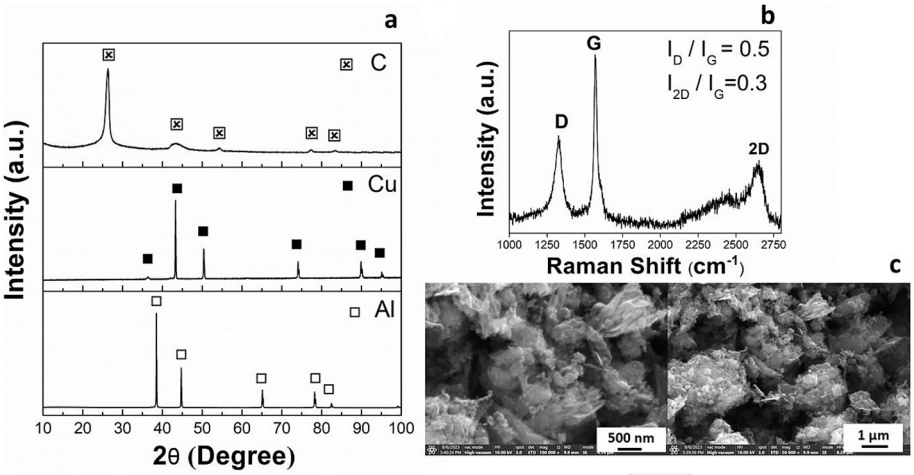

Fig. 1. a) XRD patterns of Al, Cu, and GNP powders, and b) Raman spectrum and c) SEM images of GNPs.

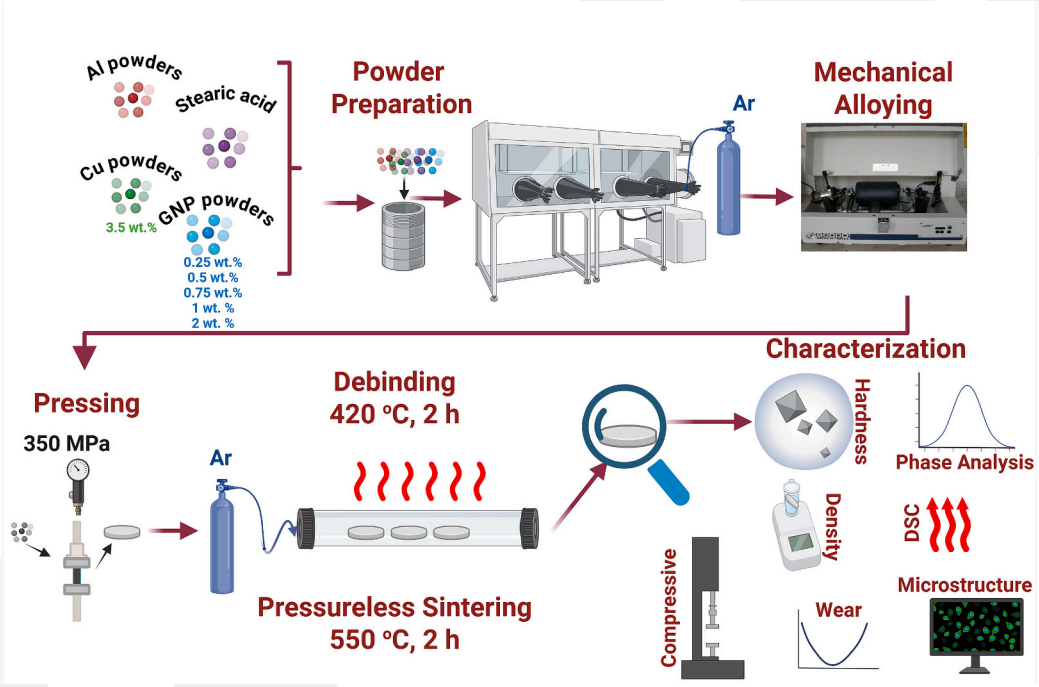

Fig. 2. Schematic illustration of experimental set-up (Created by BioRender.com).

Table 1
Compositions and mechanical alloying time of the samples with their abbreviations.

Sample	Mechanical alloying time (h)	Al-3.5 wt% Cu (wt %)	GNP (wt %)
Al3.5Cu-as-blended	0	100	–
Al3.5Cu	4	100	–
Al3.5Cu-0.25GNP	4	99.75	0.25
Al3.5Cu-0.5GNP	4	99.5	0.5
Al3.5Cu-0.75GNP	4	99.25	0.75
Al3.5Cu-1GNP	4	99	1
Al3.5Cu-2GNP	4	98	2

3. Results and discussion

XRD patterns of the as-blended Al3.5Cu and 4 h mechanically alloyed Al3.5Cu, Al3.5Cu-0.25GNP, Al3.5Cu-0.5GNP, Al3.5Cu-0.75GNP, Al3.5Cu-1GNP, and Al3.5Cu-2GNP powders are presented in Fig. 3a and b. There is no trace for GNP phase at the reinforced samples because of its low crystallinity and low amount compared to Al at the final composition [16,39,40]. Also, the reinforcement amounts are lower than the detection limit (nearly 2 wt%) of XRD. All XRD patterns show the existence of Al phase whose peaks are located around 2θ=38.5, 44.5, 65, 78, and 83° and represent diffraction from (111), (200), (220), (311), and (222) planes, respectively. Moreover, the peaks belonging to the Cu phase placed around 43 and 50° are more visible at as-blended and milled Al3.5Cu powder than those of the reinforced ones within the detection limits. Intermetallic formation and contamination could not detected within the detection limits of XRD based on the patterns of all powders. Average crystallite size and lattice strain values were

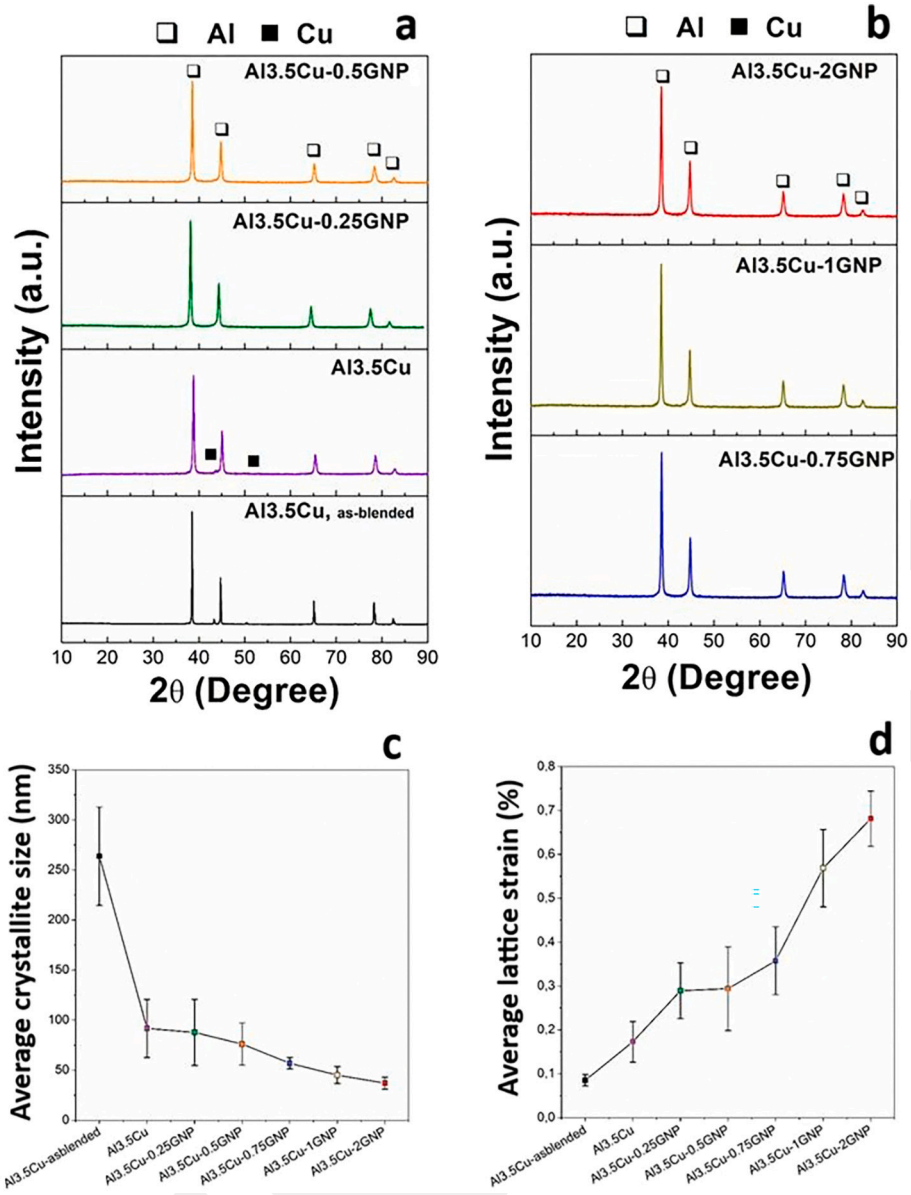

Fig. 3. a, b) XRD patterns, c) Average crystallite sizes and d) Average lattice strains of as-blended and mechanically alloyed Al3.5Cu and those GNP reinforced powders.

determined based on three most intense Al peaks and are given in Fig. 3c and d. Average crystallite size of Al3.5Cu-as-blended, Al3.5Cu, Al3.5Cu-0.25GNP, Al3.5Cu-0. 5GNP, Al3.5Cu-0.75GNP, Al3.5Cu-1GNP and Al3.5Cu-2GNP are 263.76 ± 49.1, 91.8 ± 29, 87.8 ± 33, 76.2 ± 21, 57 ± 5.8, 45.2 ± 8.4, 37.1 ± 6 nm, respectively. Average lattice strain of Al3.5Cu-as-blended, Al3.5Cu, Al3.5Cu-0.25GNP, Al3.5Cu-0. 5GNP, Al3.5Cu-0.75GNP, Al3.5Cu-1GNP and Al3.5Cu-2GNP are 0.08516 ± 0.01278, 0.17307 ± 0.04633, 0.28935 ± 0.12551, 0.29407 ± 0.1173, 0.35754 ± 0.13814, 0.56868 ± 0.06322, 0.68133 ± 0.06268 %, respectively. There is a dramatic decrease in crystallite size (263.76 ± 49.1 nm to 91.8 ± 29 nm) with 4 h milling. Lattice strain increased nearly 2 times by the effect of 4 h milling. Plastic deformations during milling led to strain increasing and crystallite size reduction [11,41,42]. Şenyurt et al. [41] mentioned that crystallite size of 1 wt% few layered graphene reinforced Al-5.5 wt% Cu powders reduced nearly 200 nm to 44 nm with 4 h MA. Also, crystallite size of the 4 h milled 1 wt% GNP reinforced Al3.5Cu composite powders that obtained in this study is 45.2 nm, and approximately the same value reported in the literature was obtained in this study for similar compositions. Increasing the amount of reinforcement led to further crystallite size reduction and lattice strain increase. The average crystallite size decreased from 91 to 37 nm, and lattice strain increased from 0.17 to 0.68 % with 2 wt% GNP-addition into Al—Cu matrix alloy. Balci et al. [42] also show a similar tendency that explains the increasing reinforcement amount into Al matrix led to crystallite size reduction and lattice strain increment.

Representative DSC thermograms belong to as-blended Al3.5Cu matrix alloy and 4 h milled Al3.5Cu-2GNP powders are presented in Fig. 4a. The endothermic peaks located at 656.27 and 639.41 °C for as-blended Al-3.5Cu and Al3.5Cu-2GNP powders, respectively. Peaking point of 656.27 °C represents the melting point of the Al. DSC thermogram of the mechanically alloyed Al3.5Cu-2GNP powders has an endothermic peak at 639.41 °C. These high intense peaks stated the melting point of proeutectic α-Al phase based on the Al—Cu binary phase diagram [43]. This melting point confirms the solubility of the Cu in the pure Al matrix via MA. The peak shifts to lower temperatures when compared to the as-blended ones. Here, there is a leftward shift in the DSC peak with the reinforcement material. Şenyurt et al. [41] also observed a leftward shift in the peaks relative to the matrix when they

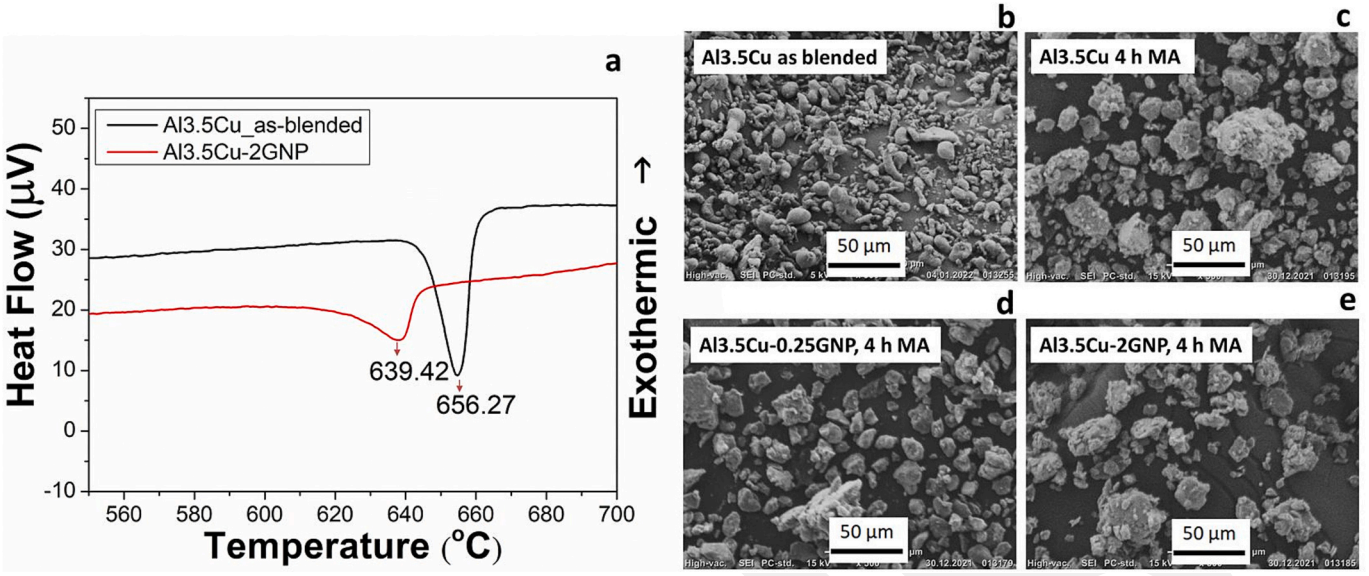

Fig. 4. a) DSC thermograms of the as-blended Al3.5Cu matrix alloy and 4 h mechanically alloyed Al3.5Cu-2GNP powders, and SEM images of b) as-blended Al3.5Cu, and 4 h mechanically alloyed c) Al3.5Cu, d) Al3.5Cu-0.25GNP and e) Al3.5Cu-2GNP powders.

added few-layered graphene reinforcement to the Al-5.5 wt% Cu matrix. The shift in the peaks increased as the amount of reinforcement material by weight increased due to the changing of lattice strain and crystallite size. Different studies have observed a shift in peaks after MA [16,34,38]. Based on the DSC thermograms, sintering temperature was determined as 550 °C. Akçamlı et al. [34] found an endothermic peak around 660 °C at DSC thermograms of Al-2GNP powders, so sintering temperature was selected as 600 °C. Furthermore, Süzer et al. [38] obtained the endothermic peaks between 647 and 651 °C at DSC thermograms of GNP-reinforced recycled Al alloy with different amounts of GNP (0–1 wt%), and there is a slight increase at their thermograms from 600 °C. Therefore, Süzer et al. [38] selected the sintering temperature as 590 °C that is the temperature below their melting points. Additionally, the absence of any other peaks may indicate that no interface was formed between Al and graphene after milling [34] within the detection limits.

SEM images of the as-blended Al3.5Cu and 4 h mechanically alloyed Al3.5Cu, Al3.5Cu-0.25GNP, and Al3.5Cu-2GNP powders are given in Fig. 4b,c,d, and e. The morphology of the as-blended powders (Fig. 4b) was completely different than the milled ones (Fig. 4c–e) with their ductile irregular shapes. However, the morphology changed to semi-equiaxed particles after 4 h milling. This difference originated from the repeated welding, fracturing and rewelding during MA [34]. During the MA of powder mixtures containing Al, Cu and GNP powders, reinforcement materials were embedded and homogeneously distributed into the matrix, so they were not seen individually at the microstructure [10]. Khanna et al. [44] mentioned that the GNPs were coated with Al matrix during the ball milling. Well-dispersed reinforcement nanoparticles led to a perfect mechanical bond between matrix and reinforcement materials [34].

Sintered compacts from as-blended Al3.5Cu, and 4 h mechanically alloyed Al3.5Cu, Al3.5Cu-0.25GNP, Al3.5Cu-0.5GNP, Al3.5Cu-0.75GNP, Al3.5Cu-1GNP, and Al3.5Cu-2GNP samples were characterized using XRD for 2θ range from 10 to 90 °C (Fig. 5a–b). Similar to the XRD patterns of powders, no peaks observed belong to GNP within the detection limits of XRD. Additionally, based on the peaks located around 20.5, 29.2, 37, 42.3, 47 and 47.6°, consistency of the Al_2Cu phase was clearly seen with the highly intense Al peaks. Additionally, the magnified XRD pattern of Al3.5Cu samples shows the location of Al_2Cu peaks in detail. Formation of Al_2Cu phase after sintering of Al—Cu composites is an expected phenomenon [17,45]. Due to the solubility of Cu in the Al matrix, Cu peaks were disappeared after sintering and Al_2Cu phase occurred [17]. The degree of diffusion between Al and Cu is governed by the formation of Al_2Cu. All intermetallics in the Al—Cu system (Cu_9Al_4, $CuAl_2$, and CuAl) have negative formation enthalpies and they are thermodynamically stable. Among them, Al_2Cu (−6.1 kJ/mol) has a lower formation enthalpy and it is more likely to form at Al—Cu systems [46,47]. Phase diagram of Al—Cu system show the formation of Al_2Cu expected after 520 °C, so phase diagram confirm the formation of Al_2Cu phase at the composites sintered at 550 °C [47]. Additionally Murray et al. [43] mentioned that MA improves the solid solubility of Cu into Al matrix even though it is hard to obtain non-equilibrium phases at room temperature. In these synthesized composites both MA and sintering at 550 °C might trigger the formation of Al_2Cu intermetallic phase. Additionally, thermochemical calculations demonstrate the potential reaction between the Al and Cu (given in Fig. S1).

SEM and color SEM images at different magnifications and EDS results of representatively selected sintered composites (Al3.5Cu, Al3.5Cu-0.5GNP, Al3.5Cu-1GNP and Al3.5Cu-2GNP) are shown in Fig. 6. According to the EDS and color SEM images, it is understood that the white particles belong to the Cu phase. Similar white-colored Al_2Cu intermetallic phase regions that distributed on the Al matrix were detected at sintered Al—Cu based composites presented in literature [41]. This phase is above 15 % atomically and even up to 20 % (Al3.5Cu-2GNP, point 2 and 3). In addition, as seen in Al3.5Cu, the matrix belongs entirely to Al. The Cu phase exhibits a semi-homogeneous and partially irregular distribution on Al. Carbon-containing regions were encountered in Al3.5Cu-0.5GNP, and these regions are attributed to the GNP reinforcement. The fact that the carbon phase could not be detected in the XRD phase indicates that it is below 2 % by weight. In addition, carbon was detected regionally in an irregular manner. It can be said that the dark areas in the composites contain GNP reinforcement.

SEM images (both with low and high magnifications) of the fracture surfaces of Al3.5Cu (a-d) and Al3.5Cu-2GNP (e-g) are demonstrated in Fig. 7 to explain the interphase existence with EDS analyses. Fig. 7a–c presents the position of Fig. 7d, which is the EDS-conducted area for the Al3.5Cu composite. While point A contains 74.7 wt% Al and 25.3 wt% Cu, dark colored point B contains 35.5 wt% Al and 64.5 wt% Cu. Point B might be interphase region with different contrast. As a representation of the Al_2Cu phase formed between Al and Cu in different studies conducted in literature, the phase formed between Al and Cu was seen to have different contrasts [5,48–51]. Li et al. [5] mentioned that strip-

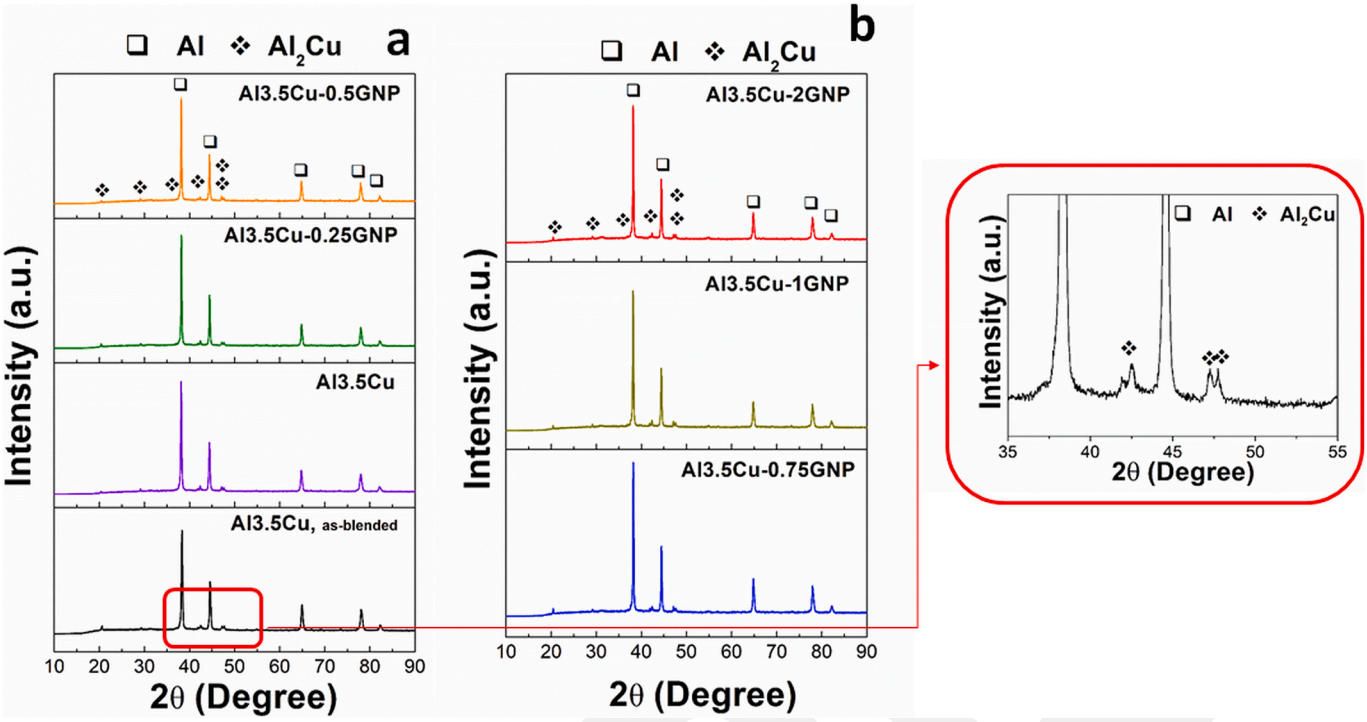

Fig. 5. XRD patterns of the sintered samples: a) Al3.5Cu as-blended, Al3.5Cu, Al3.5Cu-0.25GNP, Al3.5Cu-0.5GNP and b) Al3.5Cu-0.75GNP, Al3.5Cu-1GNP, Al3.5Cu-2GNP. (Zoom-in XRD pattern representing the Al_2Cu phase formation for the as-blended and sintered Al3.5Cu sample is also inserted.)

shaped Al_2Cu interphase placed at grain boundaries, also Fig. 7c and d exhibit similar strip-shaped formations with different contrasts. Wasik et al. [52] explain the Al_2Cu precipitates located at the grain boundaries based on EDS results that show the Cu-rich areas. Myapati et al. [51] also show the blurred region between Al and Cu-rich phases, so Fig. 7c has a blurred interface between matrix and Al_2Cu. When the GNP-reinforced composites' fracture surfaces were investigated by SEM (Fig. 7e–g), similar regions were detected (Fig. 7g) at magnified SEM images with different contrast, as explained in Fig. 7d.

Table 2 shows the density measurements of as-blended and sintered Al3.5Cu, 4 h mechanically alloyed and sintered Al3.5Cu, Al3.5Cu-0.25GNP, Al3.5Cu-0.5GNP, Al3.5Cu-0.75GNP, Al3.5Cu-1GNP, and Al3.5Cu-2GNP samples. The highest relative density was obtained from as-blended and sintered Al3.5Cu matrix sample (96.85 %). The addition of reinforcement materials reduced the density of sintered samples in the reported previous Al—Cu alloys [17,53]. Relative densities of 4 h mechanically alloyed and sintered Al3.5Cu, Al3.5Cu-0.25GNP, Al3.5Cu-0.5GNP, Al3.5Cu-0.75GNP, Al3.5Cu-1GNP, and Al3.5Cu-2GNP samples are 91.65, 93.05, 93.47, 92.68, 93.04 and 95.19 %, respectively. Among the 4 h mechanically alloyed and sintered ones, the highest density value was obtained from the Al3.5Cu-2GNP samples (95.19 %). Otherwise, there is no significant difference between the density values of sintered samples reinforced with different amounts of GNP that were milled at the same time due to weak bonds [34]. According to Akçamlı et al. [34], density values of 4 h milled and pressureless sintered 0.5, 1 and 2 wt% GNP-reinforced Al composites were 90.23, 90.30, 89.03 %, respectively. These density values were close to the measured GNP-reinforced AlCu matrix composites. GNPs has tendency to agglomeration, so mechanical alloying helps to GNPs and secondary phases to be distributed well in the microstructure and thusthe density gradually changed up to 2 GNP addition. In this study, theoretical densities were calculated according to the composite rule of mixture. However, secondary phases or porosities formed are not considered here, although they directly affect the density values. The exact determination of secondary phase amount could not be possible by applying Rietveld method due to their peak intensities.

To determine the mechanical properties of matrix alloys and composites, hardness, sliding wear tests and compression tests were performed. Microhardness values, measured with a 25 g test load, of matrix alloys and composites are presented in Fig. 8a. The as-blended and sintered matrix alloy has the lowest hardness value (104.51 ± 7.79 HV) among the sintered samples. The highest hardness value (153.55 ± 15.14 HV) was acquired from Al3.5Cu-2GNP composite. Hardness value of 4 h mechanical alloyed and sintered Al3.5Cu, Al3.5Cu-0.25GNP, Al3.5Cu-0.5GNP, Al3.5Cu-0.75GNP, Al3.5Cu-1GNP samples are 120.81 ± 9.12, 135.15 ± 9.12, 138.2 ± 12.32, 146.3 ± 17.47, 150.3 ± 16.26 HV, respectively. Mechanically alloyed and sintered Al3.5Cu samples are 1.15 times harder than the as-blended and sintered ones. Strain hardening during mechanical alloying led to hardness increase [29,31]. Increasing amount of GNP reinforcement increase the hardness of sintered composites. There is a remarkable hardness increase up to the 1 wt% reinforcement because there is a shallow increase between 1 wt% and 2 wt% reinforced ones. Moreover, uniformly distributed Al_2Cu and GNP phases improve the hardness of the composites by blocking the dislocation motions [54,55]. Hardness tests for 4 h milled and sintered Al3.5Cu-1GNP matrix alloy were applied using different loads (25 g, 50 g, 100 g, 200 g, 300 g, 500 g, 1 kg, 2 kg) and the average hardness values with standard deviations and indentation tracks' optical microscope images (using Carl Zeiss Axiolab-5 microscope) are presented in Fig. 8b, representatively. These measurements were carried out to show the effect of Vickers load on hardness values. Increasing the applied load reduced the average hardness values.

Fig. 9a demonstrates the wear volume rates with standard deviations and wear resistances of sintered samples. Wear volume losses of as-blended and sintered Al3.5Cu, 4 h mechanically alloyed and sintered Al3.5Cu, Al3.5Cu-0.25GNP, Al3.5Cu-0.5GNP, Al3.5Cu-0.75GNP, Al3.5Cu-1GNP, Al3.5Cu-2GNP samples are 2.511 ± 0.362, 0.907 ± 0.105, 0.316 ± 0.017, 0.291 ± 0.03, 0.222 ± 0.01, 0.207 ± 0.021 and 0.218 ± 0.01 mm^3. As-blended and sintered Al3.5Cu sample had the highest wear rate (25.11 ± 3.62 $mm^3/N.m \times 10^{-3}$) when it compared to the all sintered samples. Among the 4 h milled and sintered samples, Al3.5Cu sample had the highest wear rate (9.07 ± 1.05 $mm^3/N.m \times$

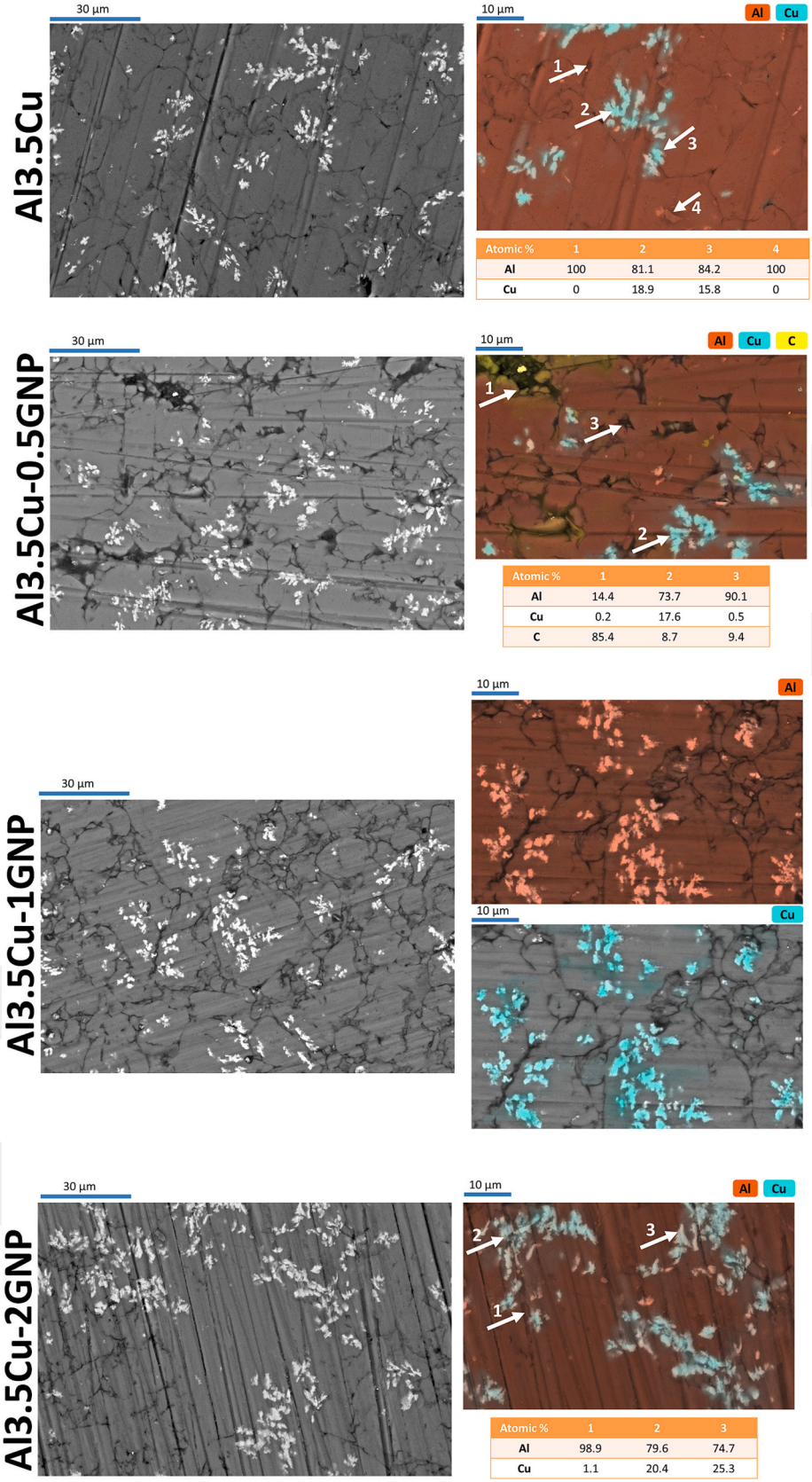

Fig. 6. SEM and color SEM images and EDS results of the representative sintered samples.

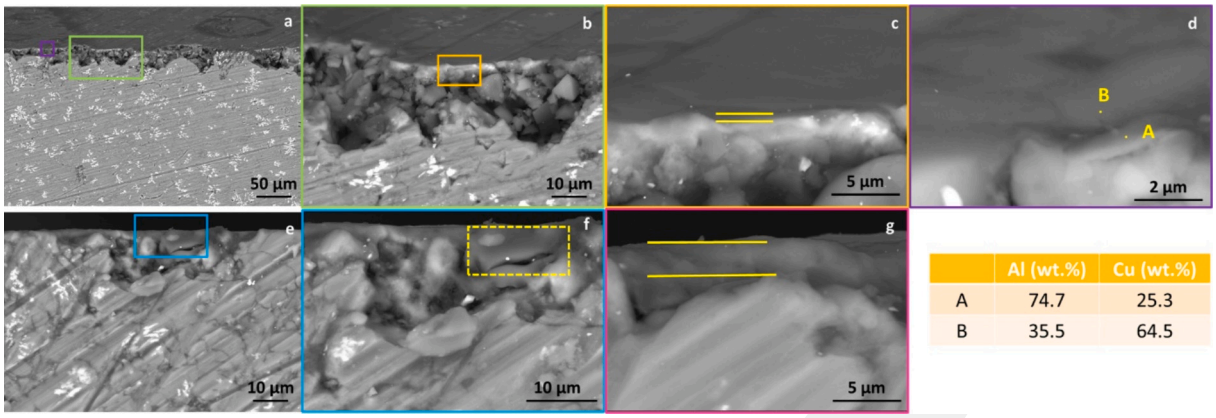

Fig. 7. SEM images with representative EDS results of fracture surfaces of Al3.5Cu (a–d) and Al3.5Cu-2GNP (e–g).

Table 2
Archimedes density measurements and relative densities of sintered samples.

Sample	Archimedes density (g/cm^3)	Relative density (%)
Al3.5Cu-as-blended	2.63	96.85
Al3.5Cu	2.49	91.65
Al3.5Cu-0.25GNP	2.52	93.05
Al3.5Cu-0.5GNP	2.53	93.47
Al3.5Cu-0.75GNP	2.50	92.68
Al3.5Cu-1GNP	2.51	93.04
Al3.5Cu-2GNP	2.50	95.19

10^{-3}). When these two matrix alloy samples (both as-blended and milled) are examined, it is seen that the wear resistance increases 2.8 times with 4 h mechanical alloying. Deaquino-Lara et al. [55] mentioned that the wear rate depends on the grain size; reduction in grain size increases the wear resistance of samples. Therefore, mechanical alloying led to grain size reduction and phases were homogeneously distributed into the microstructure, and wear resistance was improved. Adding of 0.25, 0.5, 0.75, 1 and 2 wt% GNP, wear rates are obtained as 3.16 ± 0.17, 2.91 ± 03, 2.22 ± 0.1, 2.07 ± 0.21 and 2.18 ± 0.1 $mm^3/N.m \times 10^{-3}$, respectively. The highest wear resistance was obtained with wear rate of 2.07 ± 0.21 $mm^3/N.m \times 10^{-3}$ for Al3.5Cu-1GNP composite. Wear resistance of the composites improved nearly 12 times both 1 wt% GNP addition and 4 h mechanical alloying. Following this the highest wear resistant sample, 0.75 and 2 wt% GNP reinforced composites were also showed 11 times the wear resistance compared with as-blended and sintered Al3.5Cu matrix alloy. An increasing amounts of GNP could act as a lubricant and might be caused the carbide formations [34,56]. However, up to 2 wt% GNP addition did not negatively affect the wear resistance of Al3.5Cu based composites based on the wear analyses.

Fig. 9b shows the stereo microscope images of wear tracks of as-blended and sintered Al3.5Cu, 4 h mechanically alloyed and sintered Al3.5Cu, Al3.5Cu-0.25GNP, Al3.5Cu-0.5GNP, Al3.5Cu-0.75GNP, Al3.5Cu-1GNP, Al3.5Cu-2GNP samples. Wear tracks confirm the wear volume loss values given in Fig. 9a. Whereas the narrowest wear track was observed 4 h milled and sintered Al3.5Cu-1GNP samples, the deepest and broadest wear track was detected as-blended and sintered Al3.5Cu sample. Detailed wear tracks were investigated using SEM and SEM images with EDS results of representative samples (as-blended and sintered Al3.5Cu and 4 h milled and sintered Al3.5Cu-0.5GNP) are presented in Fig. 9c and d. Deep groves, debris and delaminated parts were seen from the SEM images of the Al3.5Cu sample's wear track (Fig. 9c). EDS analyses of worn surface show the existence of 9.95 wt% Al, 1.57 wt% Cu and 4.48 wt% O. During the sliding wear test, the worn surface oxidized and formed hard Al-oxides, reducing the wear resistance. Because increased stress between the oxides and matrix initiates the crack formation and delamination [12]. Delaminated areas were observed from worn surface of Al3.5Cu-1GNP sample in Fig. 9d. Smaller

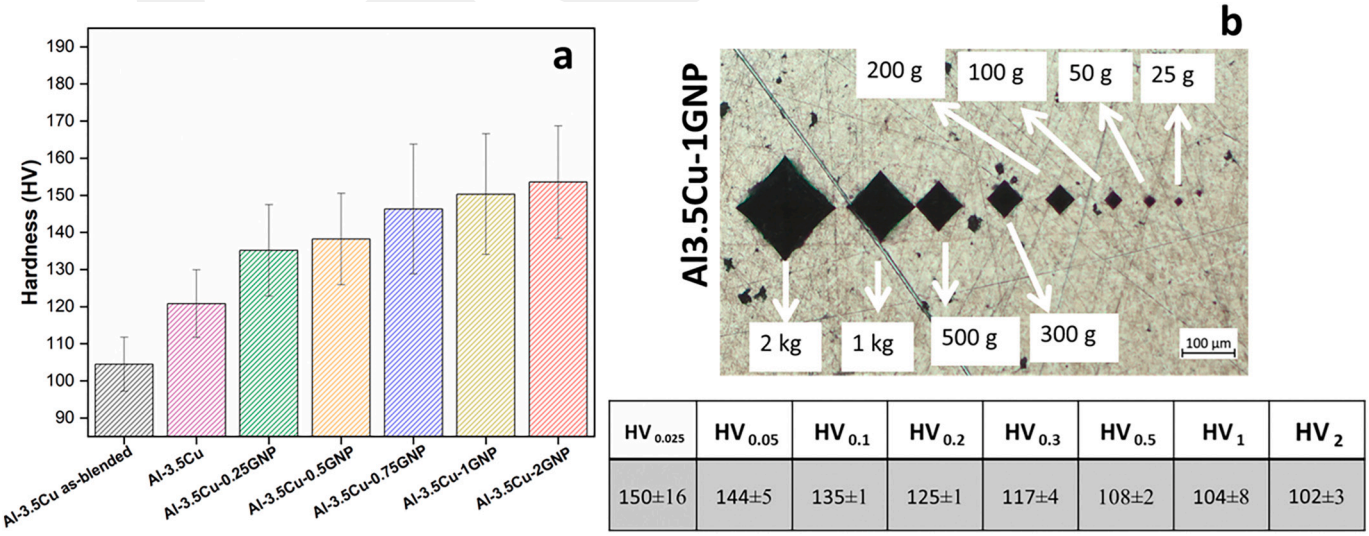

$HV_{0.025}$	$HV_{0.05}$	$HV_{0.1}$	$HV_{0.2}$	$HV_{0.3}$	$HV_{0.5}$	HV_1	HV_2
150±16	144±5	135±1	125±1	117±4	108±2	104±8	102±3

Fig. 8. a) Hardness values of sintered samples, b) Representative hardness measurements under different loads for Al3.5Cu-1GNP composite with optical microscope images of indentions.

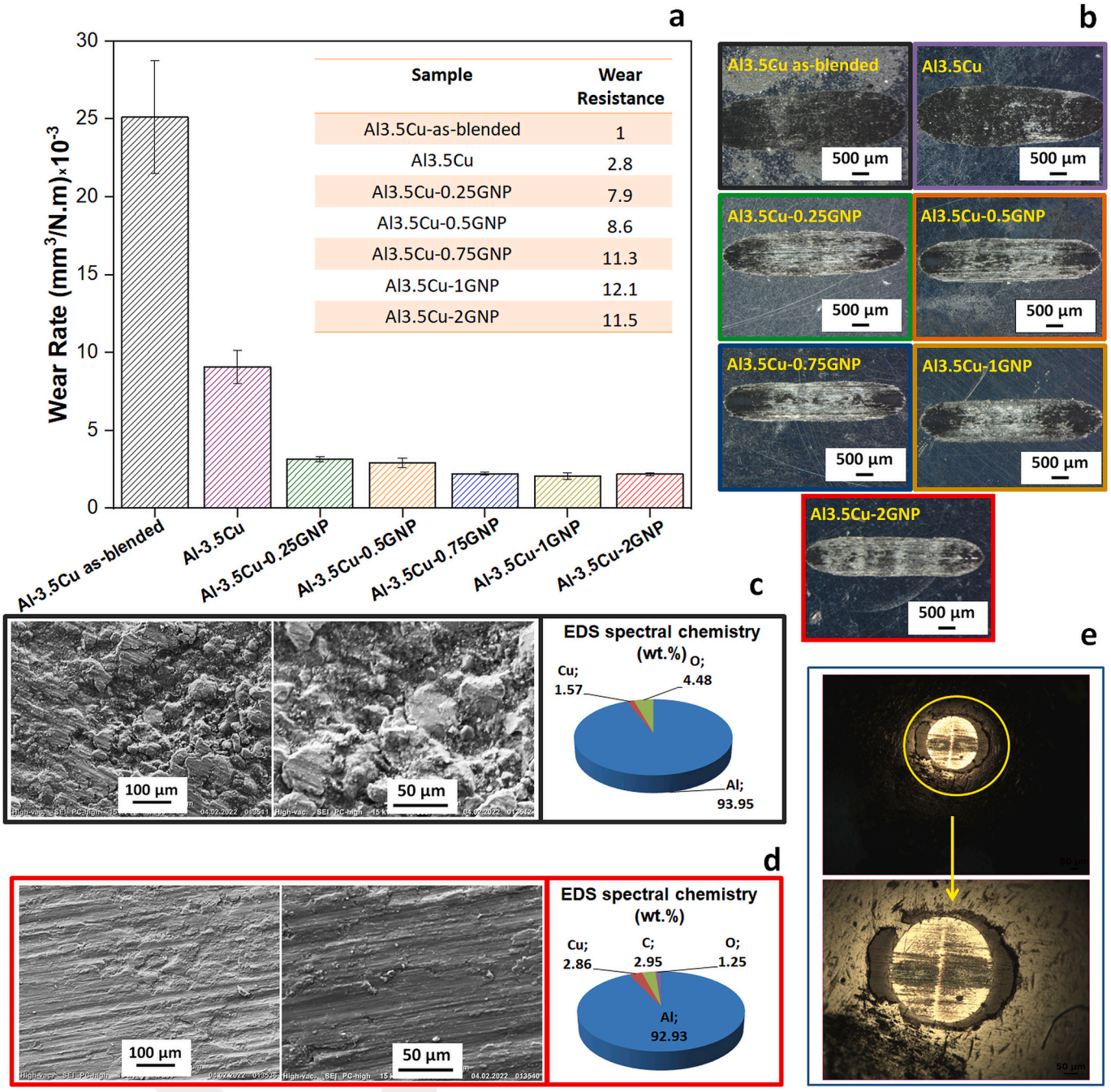

Fig. 9. a) Wear rate and wear resistance values of sintered samples, b) Stereo microscope images of wear tracks, SEM images and EDS results of c) Al3.5Cu-as-blended, d) Al3.5Cu-1GNP and d) Stereo microscope images of abrasive ball surface.

grooves are seen from Fig. 9d, that confirm the low wear rate value. Additionally, 92.93 wt% Al, 2.86 Cu, 2.95 wt% C and 1.25 wt% O content were detected using EDS analyses. Oxidation was seen during the sliding of the ball on the composite's surface, but the oxide amount was lower than the as-blended and sintered samples. Shallower grooves and delaminations are also seen from Fig. 9d, so it is possible to say that main wear mechanism is abrasive wear. Because, grooves, debris and cracks are evidence of the abrasive type of wear [12]. Additionally, formed hard oxide phases increased wear rate. Fig. 9e observed the stereo microscope image of the counter surface of the stainless steel ball after the sliding wear test with two different magnifications. Dark-colored areas were clearly seen in the middle of the ball as a line, which confirms that the sample was transferred onto the ball. Wakhi Anuar et al. [57] mentioned that both abrasive and adhesive wear mechanisms were occur simultaneously at the Al-based metal matrix composites. Therefore, dark colored adhesive parts were also confirming the adhesive wear mechanism.

The hard reinforcement particles made the matrix brittle is expected to decrease the wear rate or increase the hardness value, as seen here [58]. Another theory states that the graphene reinforcements' grain boundary pinning results in grain refinement, which increases the composite's strength by reducing dislocation motion across the Al matrix and graphene interface [44]. In addition, the homogeneous distribution of GNP without agglomeration also positively affects the mechanical properties. Morever, it can be said that the GNP reinforcement has a lubricating effect on Al, thus exhibiting a positive behavior on the wear rate. The regular clustering of GNP particles also allows the wear rate to decrease with the amount of reinforcement [59]. In their

study, Akçamlı et al. [34] related the wear rate values to agglomeration, the lubricating property of GNP and the hardness values of the material. On the other hand, the fine grains of secondary phases and matrix alloy, high densification rate, low porosity, and uniform dispersion of graphene nanoplatelets, which also have a lubricating effect in the Al matrix composites, lower the wear rate of an in-situ MA [16]. Furthermore, in comparison to the composite material, graphene, which creates a smooth tribo-layer, increases wear resistance [60]. Additionally, due to weak bonding to the matrix phase and particle clustering, the excess graphene concentration decreases wear characteristics [59]. The transformation of GNP to more brittle graphite also reduces the mechanical properties [61]. According to El-Ghazaly et al. [59], the irregular distribution of clustered GNPs in the Al matrix forms a tribolayer, which increases the wear rate. In this study, it is thought that the presence of secondary phases, the amount of porosity, and the distribution of GNP may directly affect the mechanical properties.

Compressive stress-strain plots of as-blended and sintered Al3.5Cu (Fig. 10a) and 4 h milled and sintered Al3.5Cu-0.5GNP, Al3.5Cu-0.75GNP, Al3.5Cu-1GNP, Al3.5Cu-2GNP (Fig. 10b) composites are presented. Moreover, maximum compressive stress values of composites are given in Fig. 10c. Lower ultimate compressive strength value (32.4 MPa) was detected at as-blended and sintered Al3.5Cu samples compared to other 4 h milled and GNP reinforced samples. The highest compressive strength (68.5 MPa) was acquired for Al3.5Cu-1GNP composite. Also, compressive strength of Al3.5Cu-0.5GNP, Al3.5Cu-0.75GNP, and Al3.5Cu-2GNP were 45.9, 58.0 and 64.7 MPa, respectively. The increase in compressive strength with the addition of reinforcements and milling can be attributed to Hall-Petch effect that led the uniform distribution of reinforcement particles [54,56]. Furthermore, reducing crystallite size and uniformly distributed reinforcements act as obstacles limit the dislocation motion, inhibit the fracturing and improve the strength [27,57]. Khanna et al. [44] found the 70 MPa compression strength for 1 wt% GNP-reinforced Al composites, so the results in this study are in a comparable range. Khanna et al. [44] also improved the pure Al's compression strength by adding GNP as reinforcement. After the certain amount of reinforcement led to agglomeration and cluster formations that reduce the mechanical strength of composites [44]. Therefore, 2 wt% GNPaddition slightly reduces the strength of composite.

4. Conclusions

Powder blending, mechanical alloying, cold pressing, and pressureless sintering were applied to produce matrix alloys and composites.

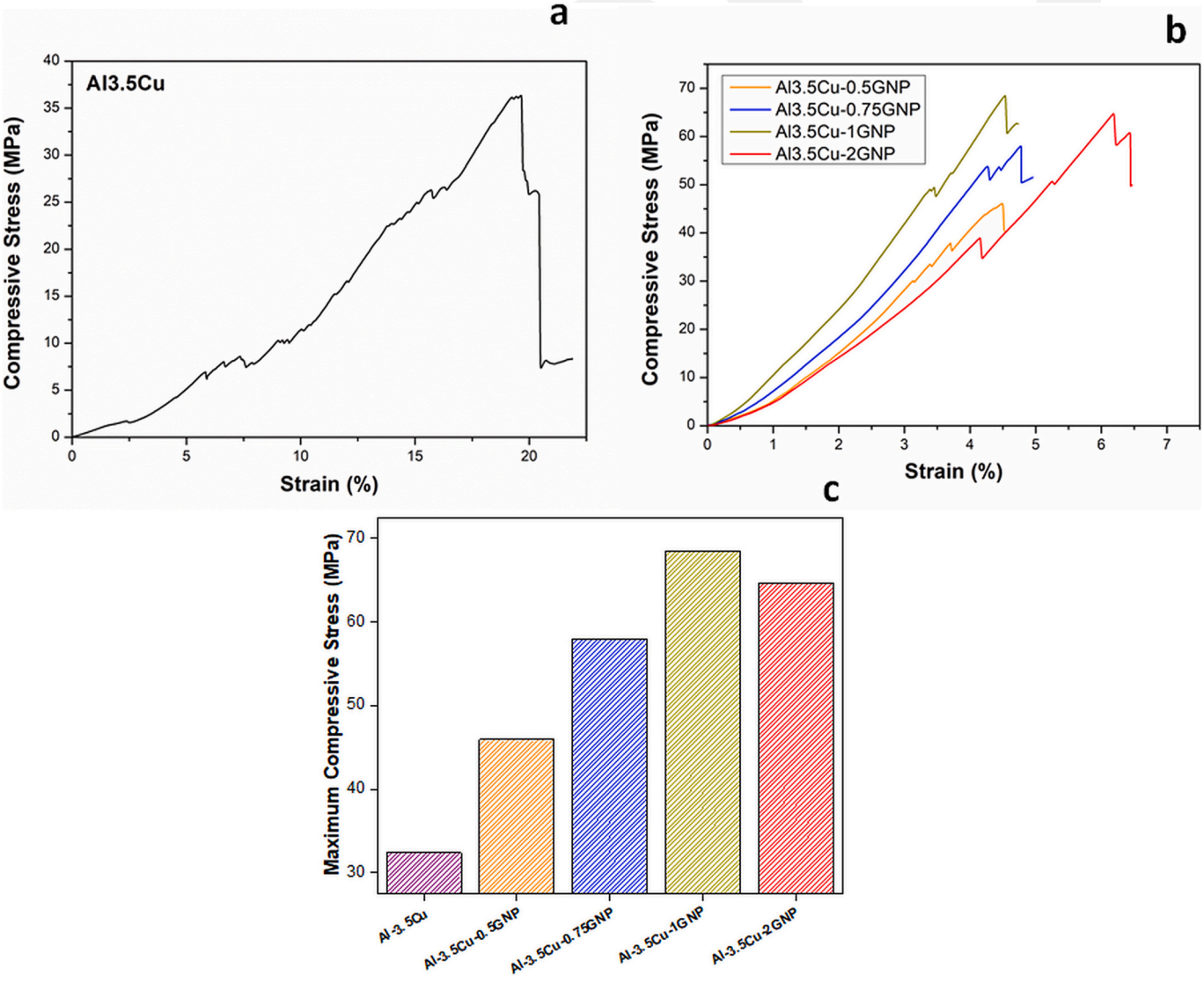

Fig. 10. Compressive stress–strain curve of a) as-blended and sintered Al3.5Cu, b) 4 h milled and sintered Al3.5Cu-0.5GNP, Al3.5Cu-0.75GNP, Al3.5Cu-1GNP and Al3.5Cu-2GNP samples, c) Maximum compressive stress values of samples.

Compared to the non-milled and sintered samples, mechanical properties were improved via mechanical alloying due to the homogeneous distribution of phases. Moreover, increasing the GNP reinforcement amount up to 1 wt % improves the mechanical properties of samples.

- According to microstructural investigations, mechanical alloying provides a uniform distribution of the phases. This uniformity is essential in improving mechanical properties of composites. In the detection limits of XRD, only Al and Al_2Cu phases were detected without oxides, carbides, or impurities at the XRD patterns of sintered samples. Al_2Cu phase formed after sintering at all milled/non-milled and sintered samples.
- Relative densities of sintered composites that measured by Archimedes' method change between 91.65 and 96.85 %. No dramatic density differences exist between the different amounts of GNP reinforced sintered composites.
- The highest Vickers microhardness value (153.55 ± 15.14 HV) was acquired from 2 wt% GNP reinforced Al3.5Cu composite. Also, the average microhardness value of 1 wt% GNP reinforced composites is around 150 HV. The hardness of the composites improved with increasing GNP amount.
- Among the sintered composites, the highest wear resistance was detected at 1 wt% GNP reinforced Al3.5Cu composite (with the lowest wear rate 2.07 ± 0.2 mm^3/N.m × 10^{-3}). The wear performance of composites was enhanced nearly 12 times with both mechanical alloying and 1 wt% GNP addition.
- Compression test results show the compression strength increases with increasing reinforcement amounts up to 1 wt%. The highest compressive strength was acquired for Al3.5Cu-1GNP composite (68.5 MPa).

To sum up, 1 wt% GNP reinforcement improves mechanical properties of Al3.5Cu-based composites; excess amount of GNP usage (over 2 wt%) probably reduced the mechanical strength due to clustering or formation of other secobdary phases.

Supplementary data to this article can be found online at https://doi.org/10.1016/j.diamond.2025.112493.

CRediT authorship contribution statement

Sıddıka Mertdinç-Ülküseven: Writing – original draft, Investigation, Formal analysis. **İlayda Süzer:** Writing – review & editing, Formal analysis. **Ahmet Kasım Ürper:** Formal analysis. **Alper İbrahim Çelik:** Investigation. **Doruk Tuncer Baci:** Investigation. **Kerem Alper Gürarslan:** Investigation. **M. Lütfi Öveçoğlu:** Writing – review & editing, Conceptualization. **Duygu Ağaoğulları:** Writing – review & editing, Writing – original draft, Supervision, Conceptualization.

Declaration of competing interest

The authors declare that they have no known competing financial interests or personal relationships that could have appeared to influence the work reported in this paper.

Acknowledgements

The authors thank to Istanbul Technical University Scientific Research Projects Department for supporting this study with the project number of MGA-2023-44054. The authors thank to Prof. Dr. Hüseyin Çimenoğlu, Dr. Faiz Muhaffel, Assoc. Prof. Dr. Nazlı Akçamlı-Kaya and M.Sc. Berk Şenyurt for their helps during mechanical and thermal tests.

Data availability

Data will be made available on request.

References

[1] A. Zotti, S. Zuppolini, A. Borriello, M. Zarrelli, Polymer nanocomposites based on graphite Nanoplatelets and amphiphilic graphene platelets, Compos. Part B Eng. 246 (2022) 110223, https://doi.org/10.1016/j.compositesb.2022.110223.
[2] X. Li, J. Yu, S. Wageh, A.A. Al-Ghamdi, J. Xie, Graphene in Photocatalysis: a review, Small 12 (2016) 6640–6696, https://doi.org/10.1002/smll.201600382.
[3] A.K. Geim, K.S. Novoselov, The rise of graphene, Nat. Mater. 6 (2007) 183–191, https://doi.org/10.1038/nmat1849.
[4] Z. Zhen, H. Zhu, Structure and properties of graphene, Elsevier Inc., 2017, pp. 1–12, https://doi.org/10.1016/B978-0-12-812651-6.00001-X.
[5] M. Li, W. Yang, X. Tian, L. Chen, H. Hou, Y. Zhao, Precipitation and refining of Al_2Cu in graphene nanoplatelets reinforced 2024 Al composites, Mater Charact 200 (2023) 112854, https://doi.org/10.1016/j.matchar.2023.112854.
[6] M. Bahiraei, S. Heshmatian, Graphene family nanofluids: a critical review and future research directions, Energ. Conver. Manage. 196 (2019) 1222–1256, https://doi.org/10.1016/j.enconman.2019.06.076.
[7] A. Jiménez-Suárez, S.G. Prolongo, Graphene nanoplatelets, Appl. Sci. 10 (2020) 1753, https://doi.org/10.3390/app10051753.
[8] S. Xiang, X. Wang, M. Gupta, K. Wu, X. Hu, M. Zheng, Graphene nanoplatelets induced heterogeneous bimodal structural magnesium matrix composites with enhanced mechanical properties, Sci. Rep. 6 (2016) 38824, https://doi.org/10.1038/srep38824.
[9] P. Cataldi, A. Athanassiou, I.S. Bayer, Graphene nanoplatelets-based advanced materials and recent progress in sustainable applications, Appl. Sci. 8 (2018) 1438, https://doi.org/10.3390/app8091438.
[10] R. Pérez-Bustamante, D. Bolaños-Morales, J. Bonilla-Martínez, I. Estrada-Guel, R. Martínez-Sánchez, Microstructural and hardness behavior of graphene-nanoplatelets/aluminum composites synthesized by mechanical alloying, J. Alloys Compd. 615 (2015) S578–S582, https://doi.org/10.1016/j.jallcom.2014.01.225.
[11] D. Ağaoğulları, Effects of ZrC content and mechanical alloying on the microstructural and mechanical properties of hypoeutectic Al-7 wt.% Si composites prepared by spark plasma sintering, Ceram. Int. 45 (2019) 13257–13268, https://doi.org/10.1016/j.ceramint.2019.04.013.
[12] E. Tekoğlu, D. Ağaoğulları, S. Mertdinç, A.H. Paksoy, M.L. Öveçoğlu, Microstructural characterizations and mechanical properties of NbB_2 and VB particulate-reinforced eutectic Al-12.6 wt% Si composites via powder metallurgy method, Adv. Powder Technol. 29 (2018) 2070–2081, https://doi.org/10.1016/j.apt.2018.05.013.
[13] L. Chen, Y. Qi, Y. Fei, Z. Du, Enhanced mechanical properties and thermal conductivity for GNPs/Al2024 composites with in situ SiC Nanorods, Met. Mater. Int. 27 (2021) 4263–4270, https://doi.org/10.1007/s12540-020-00803-9.
[14] S. Khoshsima, S. Mertdinç, A. Motallebzadeh, Z. Altıntaş, D. Ağaoğulları, Ö. Balcı-Çağıran, Enhanced hardness and wear resistance of Al-based hybrid MMCs by using of composite metal boride reinforcement particles, Mater. Chem. Phys. 288 (2022) 126377, https://doi.org/10.1016/j.matchemphys.2022.126377.
[15] S. Mertdinç, E. Tekoğlu, D. Ağaoğullari, M.L. Öveçoğlu, Influence of the milling process on TiB_2 particle reinforced Al-7 wt.-% Si matrix composites, Materialpruefung/Mater. Test. 60 (2018), https://doi.org/10.3139/120.111207.
[16] B. Senyurt, B. Kücükelyas, M. Bellek, S. Kavak, G. Borand, D. Uzunsoy, D. Agaogullari, N. Akcamli, Few-layered graphene reinforced Al-10 wt% Si-2 wt% cu matrix composites, J. Mater. Res. Technol. 21 (2022) 486–501, https://doi.org/10.1016/j.jmrt.2022.09.049.
[17] S. Mertdinç, M. Kılık, Ş. Baltaş, A. Kaan Taşkın, M.L. Öveçoğlu, D. Ağaoğulları, Characterization investigations of mechanically alloyed and sintered Al – 4 wt% cu matrix composites reinforced with mechanochemically synthesized chromium boride/nitride particles, Solid State Sci. 120 (2021) 106727, https://doi.org/10.1016/j.solidstatesciences.2021.106727.
[18] J. Zmywaczyk, J. Sienkiewicz, P. Koniorczyk, J. Godzimirski, M. Zieliński, Investigation of Thermophysical properties of AW-2024-T3 bare and clad aluminum alloys, Materials 13 (2020) 3345, https://doi.org/10.3390/ma13153345.
[19] P. Wang, A. Gebert, L. Yan, H. Li, C. Lao, Z. Chen, K. Kosiba, U. Kühn, S. Scudino, Corrosion of Al-3.5Cu-1.5 mg–1Si alloy prepared by selective laser melting and heat treatment, Intermetallics 124 (2020) 106871, https://doi.org/10.1016/j.intermet.2020.106871.
[20] T. Dursun, Recent developments in advanced aircraft aluminium alloys, Mater. Des. 5 (2014) 862–871, https://doi.org/10.1016/j.matdes.2013.12.002.
[21] M. Aravind, P. Yu, M.Y. Yau, D.H.L. Ng, Formation of Al2Cu and AlCu intermetallics in Al(cu) alloy matrix composites by reaction sintering, Mater. Sci. Eng. A 380 (2004) 384–393, https://doi.org/10.1016/j.msea.2004.04.013.
[22] F. Qiu, X. Gao, J. Tang, Y.-Y. Gao, S.-L. Shu, X. Han, Q. Li, Q.-C. Jiang, Microstructures and tensile properties of Al–cu matrix composites reinforced with Nano-sized SiCp fabricated by semisolid stirring process, Metals 7 (2017) 49, https://doi.org/10.3390/met7020049.
[23] S.G. Shabestari, H. Moemeni, Effect of copper and solidification conditions on the microstructure and mechanical properties of Al-Si-mg alloys, J. Mater. Process. Technol. 153-154 (2004) 193–198, https://doi.org/10.1016/j.jmatprotec.2004.04.302.
[24] J. Zhang, Z. Chen, J. Zhao, Z. Jiang, Microstructure and mechanical properties of aluminium-graphene composite powders produced by mechanical milling, Mech. Adv. Mater. Mod. Process. 4 (2018), https://doi.org/10.1186/s40759-018-0037-5.
[25] A. Saboori, S.K. Moheimani, M. Dadkhah, M. Pavese, C. Badini, P. Fino, An overview of key challenges in the fabrication of metal matrix nanocomposites reinforced by graphene nanoplatelets, Metals (Basel) 8 (2018) 172, https://doi.org/10.3390/met8030172.

[26] A. Md Ali, M.Z. Omar, H. Hashim, M.S. Salleh, I.F. Mohamed, Recent development in graphene-reinforced aluminium matrix composite: a review, Rev. Adv. Mater. Sci. 60 (2021) 801–817, https://doi.org/10.1515/rams-2021-0062.
[27] H.P. Boehm, R. Setton, E. Stumpp, Nomenclature and terminology of graphite intercalation compounds. Report by a subgroup of the International Committee for Characterization and Terminology of carbon and graphite on suggestions for rules for the nomenclature and terminology of graphite intercalation compounds, Synth. Met. 11 (1985) 363–371, https://doi.org/10.1016/0379-6779(85)90068-2.
[28] C. Lee, X. Wei, J.W. Kysar, J. Hone, Measurement of the elastic properties and intrinsic strength of monolayer graphene, Science 321 (2008) 385–388, https://doi.org/10.1126/science.1157996.
[29] C. Suryanarayana, Mechanical alloying and milling, Prog. Mater. Sci. 46 (2001) 1–184, https://doi.org/10.1016/S0079-6425(99)00010-9.
[30] İ. Süzer, Y.E. Özçakıcı, A.S. Tekinşen, K.G. Bayrak, S. Mertdinç-Ülküseven, Ö. Balcı-Çağıran, M.L. Öveçoğlu, D. Ağaoğulları, High entropy (HfTiZrVNb)B2 ceramic particulate reinforced Al matrix composites: synthesis, mechanical, microstructural and thermal characterization, Ceram. Int. 50 (2024) 26583–26595, https://doi.org/10.1016/j.ceramint.2024.04.386.
[31] K. Rashidi, M. Moazami-Goudarzi, A. Masoudi, Powder processing, characterization and mechanical properties of Al/GNP composites, Mater. Chem. Phys. 256 (2020) 123719, https://doi.org/10.1016/j.matchemphys.2020.123719.
[32] Z. Zheng, X. Yang, J.C. Li, X. Zhang, I. Muhammad, L. Geng, Preparation and properties of graphene nanoplatelets reinforced aluminum composites, Trans. Nonferrous Met. Soc. China 31 (2021) 878–886, https://doi.org/10.1016/S1003-6326(21)65546-2.
[33] M. Rashad, F. Pan, A. Tang, M. Asif, Effect of graphene Nanoplatelets addition on mechanical properties of pure aluminum using a semi-powder method, Prog. Nat. Sci. Mater. Int. 24 (2014) 101–108, https://doi.org/10.1016/j.pnsc.2014.03.012.
[34] N. Akçamli, B. Küçükelyas, C. Kaykilarli, D. Uzunsoy, Investigation of microstructural, mechanical and corrosion properties of graphene nanoplatelets reinforced Al matrix composites, Mater. Res. Express. 6 (2019) 115627, https://doi.org/10.1088/2053-1591/ab511f.
[35] Z. Zheng, X. Zhang, M. Qian, J. Li, M. Imran, L. Geng, Ultra-high strength GNP/2024Al composite via thermomechanical treatment, J. Mater. Sci. Technol. 108 (2022) 164–172, https://doi.org/10.1016/j.jmst.2021.08.056.
[36] O.A. El-Kady, H.M. Yehia, F. Nouh, I.M. Ghayad, T. El-Bitar, W.M. Daoush, Enhancement of physical properties and corrosion resistance of Al-cu-Al_2O_3/graphene nanocomposites by powder metallurgy technique, Materials (Basel) 15 (2022) 7116, https://doi.org/10.3390/ma15207116.
[37] F. Lin, F. Jia, M. Ren, J. Wang, M. Yang, Z. Chen, Z. Jiang, Microstructure, mechanical and thermal properties of ultrafine-grained Al2024–TiC-GNPs nanocomposite, Mater. Sci. Eng. A 841 (2022) 142855, https://doi.org/10.1016/j.msea.2022.142855.
[38] İ. Süzer, S.B. Hayirci, E. Boyaci, A. Deniz, S. Mertdinç-Ülküseven, M.L. Öveçoğlu, H. Gökçe, D. Ağaoğulları, Graphene Nanoplatelet reinforced Al-based composites prepared from recycled powders via mechanical alloying and Pressureless sintering, Diamond Relat. Mater. 149 (2024) 111552, https://doi.org/10.1016/j.diamond.2024.111552.
[39] E. Tekoğlu, D. Ağaoğulları, Y. Yürektürk, B. Bulut, M. Lütfi Öveçoğlu, Characterization of LaB_6 particulate-reinforced eutectic Al-12.6 wt% Si composites fabricated via mechanical alloying and spark plasma sintering, Powder Technol. 340 (2018) 473–483, https://doi.org/10.1016/j.powtec.2018.09.055.
[40] C. Suryanarayana, Mechanical alloying: a critical review, Mater. Res. Lett. 10 (2022) 619–647, https://doi.org/10.1080/21663831.2022.2075243.
[41] B. Şenyurt, K.Ç. Yaman, N. Akçamlı, Few-layered graphene/Al-cu alloy matrix composites: mechanical, Tribological and corrosion properties, Materials Today Communications 40 (2024) 110082, https://doi.org/10.1016/j.mtcomm.2024.110082.
[42] Ö. Balcı, D. Ağaoğulları, H. Gökçe, M.L. Öveçoğlu, M. Somer, Effect of Cryomilling on matrix/reinforcement interfaces and properties of Al-TiB_2 composites, J. Alloys Compd. 757 (2018) 393–402, https://doi.org/10.1016/j.jallcom.2018.05.098.
[43] J.L. Murray, The aluminium-copper system, Int. Met. Rev. 1 (1985) 27–33, https://doi.org/10.1179/imtr.1985.30.1.211.
[44] V. Khanna, V. Kumar, S.A. Bansal, C. Prakash, M. Ubaidullah, S.F. Shaikh, A. Pramanik, A. Basak, S. Shankar, Fabrication of efficient aluminium/graphene nanosheets (Al-GNP) composite by powder metallurgy for strength applications, J. Mater. Res. Technol. 22 (2023) 3402–3412, https://doi.org/10.1016/j.jmrt.2022.12.161.
[45] C.J. Hsu, P.W. Kao, N.J. Ho, Ultrafine-grained Al-Al_2Cu composite produced in situ by friction stir processing, Scr. Mater. 53 (2005) 341–345, https://doi.org/10.1016/j.scriptamat.2005.04.006.
[46] J. Tian, Y. Zhao, H. Hou, P. Han, First-principles investigation of the structural, mechanical and thermodynamic properties of Al_2Cu phase under various pressure and temperature conditions, Solid State Commun. 268 (268) (2017) 44–50, https://doi.org/10.1016/j.ssc.2017.09.016.
[47] S.N. Alam, P. Shrivastava, D. Panda, D.B. Gunale, K. Susmitha, P. Pola, Synthesis of Al_2Cu intermetallic compound by mechanical alloying, Materials Today Communications 31 (2022) 103267, https://doi.org/10.1016/j.mtcomm.2022.103267.
[48] A. Jadidi, R.B. Azhiri, A. Baghdadchi, A. Salmanibideskan, Lap joining of aluminum 5052 to copper by optimum friction stir spot welding process, Int. J. Adv. Manuf. Technol. 119 (2022) 7339–7352, https://doi.org/10.1007/s00170-021-08541-x.
[49] S. Jain, M. Patel, J. Murugesan, S. Samal, Influence of friction stir processing on novel designed Aluminium-based alloy to enhance strength and ductility, Arab. J. Sci. Eng. 49 (2024) 1969–1976, https://doi.org/10.1007/s13369-023-08063-6.
[50] H. Gao, L. Wang, S. Liu, J. Li, C. Kong, H. Yu, Effects of a stainless steel interlayer on the interfacial microstructure and bonding strength of cu/Al clad sheets prepared via the powder-in-tube method, J. Mater. Res. Technol. 15 (2021) 3514–3524, https://doi.org/10.1016/j.jmrt.2021.09.144.
[51] A. Wąsik, B. Leszczyńska-Madej, M. Madej, M. Goły, Effect of heat treatment on microstructure of Al4Cu-SiC composites consolidated by powder metallurgy technique, J. Mater. Eng. Perform. 29 (2020) 1841–1848, https://doi.org/10.1007/s11665-020-04685-1.
[52] O. Mypati, P.P. Kumar, S.K. Pal, P. Srirangam, TEM analysis and molecular dynamics simulation of graphene coated Al-cu micro joints, Carbon Trends 9 (2022) 100223, https://doi.org/10.1016/j.cartre.2022.100223.
[53] M. Sameezadeh, H. Farhangi, M. Emamy, Nanocomposites of aluminum alloy-$MoSi_2$: synthesis and characterization, J. Compos. Mater. 49 (2015) 3145–3155, https://doi.org/10.1177/0021998314560384.
[54] E. Tekoğlu, Y. Yürektürk, D. Ağaoğulları, D. Ovalı, S. Mertdinç, M. Lütfi Öveçoğlu, Characterization of mechanically alloyed and pressureless sintered Al-7 wt% Si-2 wt% LaB_6-2 wt% ($MoSi_2$, WSi_2) hybrid composites, Adv. Powder Technol. 30 (2019) 2626–2635, https://doi.org/10.1016/j.apt.2019.08.010.
[55] R. Deaquino-Lara, N. Soltani, A. Bahrami, E. Gutiérrez-Castañeda, E. García-Sánchez, M.A.L. Hernandez-Rodríguez, Tribological characterization of Al7075-graphite composites fabricated by mechanical alloying and hot extrusion, Mater. Des. 67 (2015) 224–231, https://doi.org/10.1016/j.matdes.2014.11.045.
[56] N. Akçamlı, B. Şenyurt, H. Gökçe, D. Ağaoğulları, Powder metallurgical fabrication of graphene reinforced near-eutectic Al-Si matrix composites: microstructural, mechanical and electrochemical characterization, Eng. Sci. Technol. an Int. J. 31 (2022) 101052, https://doi.org/10.1016/j.jestch.2021.08.009.
[57] N.F.B. Wakhi Anuar, M.S. Salleh, M.Z. Omar, W.F.H.W. Zamri, A. Md Ali, S. Samat, Wear properties of graphene-reinforced aluminium metal matrix composite: a review, Rev. Adv. Mater. Sci. 62 (2023) 20220326, https://doi.org/10.1515/rams-2022-0326.
[58] E.B. Moustafa, S. Abdel Aziz, M.A. Taha, A. Saber, Influence of graphene and silver addition on aluminum's thermal conductivity and mechanical properties produced by the powder metallurgy technique, Metals 13 (2023) 836, https://doi.org/10.3390/met13050836.
[59] A. El-Ghazaly, G. Anis, H.G. Salem, Effect of graphene addition on the mechanical and Tribological behavior of nanostructured AA2124 self-lubricating metal matrix composite, Compos. A: Appl. Sci. Manuf. 95 (2017) 325–336, https://doi.org/10.1016/j.compositesa.2017.02.006.
[60] M. Reihanian, S. Fayezipour, S.M. Lari Baghal, Nanostructured Al/SiC-graphite composites produced by accumulative roll bonding: role of graphite on microstructure, Wear and tensile behavior, J. of Materi Eng and Perform. 26 (2017) 1908–1919, https://doi.org/10.1007/s11665-017-2608-8.
[61] W. Tian, S. Li, B. Wang, X. Chen, J. Liu, M. Yu, Graphene-reinforced aluminum matrix composites prepared by spark plasma sintering, Int. J. Miner. Metall. Mater. 23 (6) (2016) 723–729, https://doi.org/10.1007/s12613-016-1286-0.